UCLA
UCLA Previously Published Works

Title

Understanding the influence of hydrogen pressure on the enantioselectivity of hydrogenation: A combined theory-experiment approach

Permalink

https://escholarship.org/uc/item/3wm6m1gn

Authors

Aloui, A
Delbecq, F
De Bellefon, C
et al.

Publication Date

2017-05-01

DOI

10.1016/j.jorganchem.2017.02.034

Peer reviewed

eScholarship.org Powered by the California Digital Library
University of California

Understanding the influence of hydrogen pressure on the enantioselectivity of hydrogenation: a combined theory-experiment approach.

A. ALOUI[1,2] , F. DELBECQ[2], C. De BELLEFON[1], P. SAUTET[2,3*]

Abstract

Why would the pressure of hydrogen affect the enantioselectivity of hydrogenation in an opposite way for two enamide reactants, M-acrylate (methyl 2-acetamidoacrylate) and E-emap (ethyl 4-methyl-3-acetamido-2-pentanoate), with rhodium (I) complexes coordinated to a diphosphine ligand? This question was answered by a combination of experiments and DFT calculations. The activation free energies, the kinetic constants and the enantiomeric excess *ee* have been calculated. In the static pathways, the two substrates show significant differences. From the square-planar substrate-metal complex, M-acrylate (resp. E-emap) prefers the attack of the hydrogen on the side opposite to (resp. of) the amide group. Both substrates however show lower transition states on the pathway starting from the minor stereoisomer of the substrate-metal complex. The turnover-limiting step for M-acrylate is the oxidative addition of hydrogen on the substrate-metal complex, while it is the migratory insertion of the substrate in the Rh-H bond for E-emap. However, the energy profiles are not sufficient to understand the enantioselectivity of the reaction: the kinetic simulations lead to different conclusions and show a marked influence of the hydrogen pressure. For both substrates, the R isomer is obtained in the realistic pressure range, coming from the minor isomer for M-acrylate and from the major isomer for E-emap. Hence, depending on the reactant, the preferred pathway follows either the major/minor or the lock-and-key concept. The importance of combining DFT calculations with kinetic simulations in unraveling the mechanism is underlined. In particular, they reveal that the rate of formation of the metal-substrate complex plays a key role for the enantioselectivity.

Keywords: Enantioselectivity; hydrogen pressure; DFT; Rhodium; enamide; mechanism

[1] Laboratoire de Génie des Procédés Catalytiques, CNRS-CPE Lyon, UMR 5285,
43, bd du 11 novembre 1918, B.P. 82077 - 69616 VILLEURBANNE Cedex
[2] Université de Lyon, CNRS, Laboratoire de Chimie, École normale supérieure de Lyon- 15 parvis René Descartes, BP 7000, 69342 Lyon Cedex 07, France
[3] Department of Chemical and Biomolecular Engineering, University of California, Los Angeles, Los Angeles, CA 90095, United States of America.
* sautet@ucla.edu

Introduction

The catalytic asymmetric hydrogenation is one of the most efficient and convenient methods for synthesizing optically active compounds, e.g. amino acids and chiral amines which are widely used in the pharmaceutical and fine chemical industries.[1] The fine control and optimization of the enantioselectivity is of utmost importance. In spite of the widespread use of that reaction, and of the efforts of several groups, the influence of the hydrogen pressure on the enantioselectivity is still not completely understood[2,6]. Such an effect seems to be general and an equivalent distribution between beneficial and detrimental pressure effects on ee has been demonstrated.[3] In a recent work, we have identified a very interesting catalytic system, $[Rh(R,R)Me\text{-}BPE]^+$, which gives two opposite effects of the hydrogen pressure on enantiomeric excess, depending on the substrate structure : a detrimental effect with M-acrylate, (methyl 2-acetamidoacrylate) and a beneficial effect with E-emap (ethyl 4-methyl-3-acetamido-2-pentanoate)[4], which contrasts with previous results showing pressure independent ee values for E-enamides with Duphos type ligands. [5]. For M-acrylate, the enantiomeric excess decreases from 94 to 56% with increasing the hydrogen pressure from 2 to 41 bars, whereas, a noticeable increase of enantioselectivity, from 20 to 70%, was obtained with E-emap in the same pressure range[3] (Figure 1). The product chirality was the same for the two substrates, i.e. both lead to the R product. At this point, a clarification must be done concerning the absolute configuration of the products obtained with E-emap. In our previous experimental paper, the determination was erroneous and a detailed explanation is given in the SI (part I).

This opposite influence of the pressure of hydrogen for the two reactants on the reaction enantioselectivity calls for a rationalization. Understanding the reactivity of the different reaction intermediates and combining these elementary steps in a kinetic simulation are central to elucidate the origin of the observed enantioselectivity and to understand its variation with the hydrogen pressure and substrate structure. For that purpose, theoretical chemistry is among the best tool. In particular the use of the density functional theory (DFT) becomes more and more helpful to interpret, rationalize and extrapolate the experimental data.

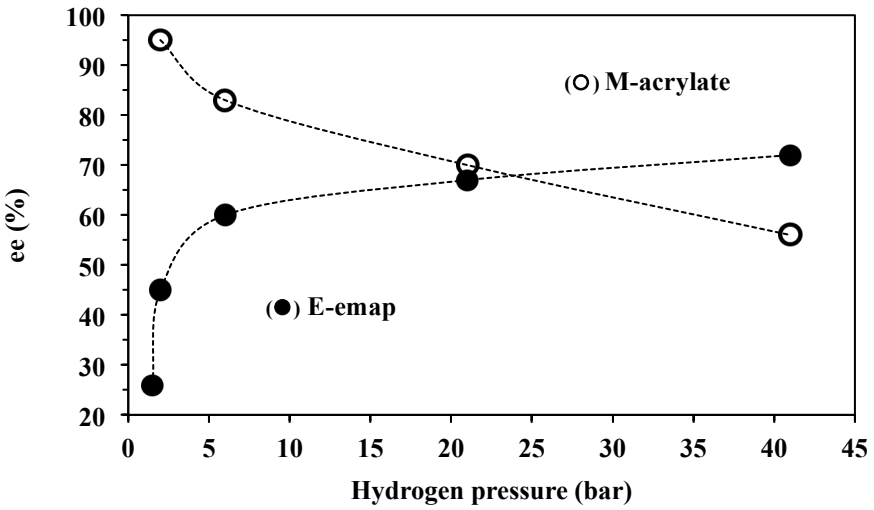

Figure 1 : Dependence of the enantiomeric excess on hydrogen pressure ([M-acrylate]= 0,1 kmol.m^{-3} ; ([E-emap] =0,1 kmol.m^{-3} ; [Rh]=10^{-3} -10^{-4} kmol.m^{-3} ; L/Rh=1,05 ; T=308 K)

The asymmetric hydrogenation with H_2, catalyzed by organometallic complexes, has been the subject of numerous experimental and theoretical studies[6]. Cationic complexes of Rh(I) have been widely used. In fact, previous mechanistic studies have led to the development of reaction schemes for the rhodium-catalyzed enantioselective hydrogenation. Two mechanisms have been proposed: the dihydride mechanism and the unsaturated mechanism. In the former, the formation of the dihydride intermediate occurs before the coordination of the substrate.[6g,h] In that case, it can be simply shown that the enantioselectivity does not generally depend on the hydrogen pressure[7]. This has led us to discard this mechanism. The second mechanism has been proposed by Halpern and Landis[6a-d] and by Brown *et al.*[8]. It has already been applied to study the influence of hydrogen pressure on a specific complex.[2d] The first step is the coordination of the prochiral substrate to the rhodium chiral diphosphine complex, leading to two diastereomeric square-planar catalyst-substrate complexes (noted SQPL in Scheme 1), depending on the used alkene enantioface for coordination. Addition of H_2 then proceeds through a trigonal bipyramidal molecular hydrogen complex (MOLH2, molh2), which is followed by the oxidative addition of H_2 to form the dihydride complex (DIHY, dihy). Then, the migratory insertion of an alkene carbon into one Rh-H bond generates an alkyl hydride (ALHY, alhy) that is further hydrogenated to alkane by the transfer of the second hydride and a reductive elimination to regenerate the catalyst (scheme 1). Some intermediates (MOLH2, ALHY) could not be directly observed experimentally.

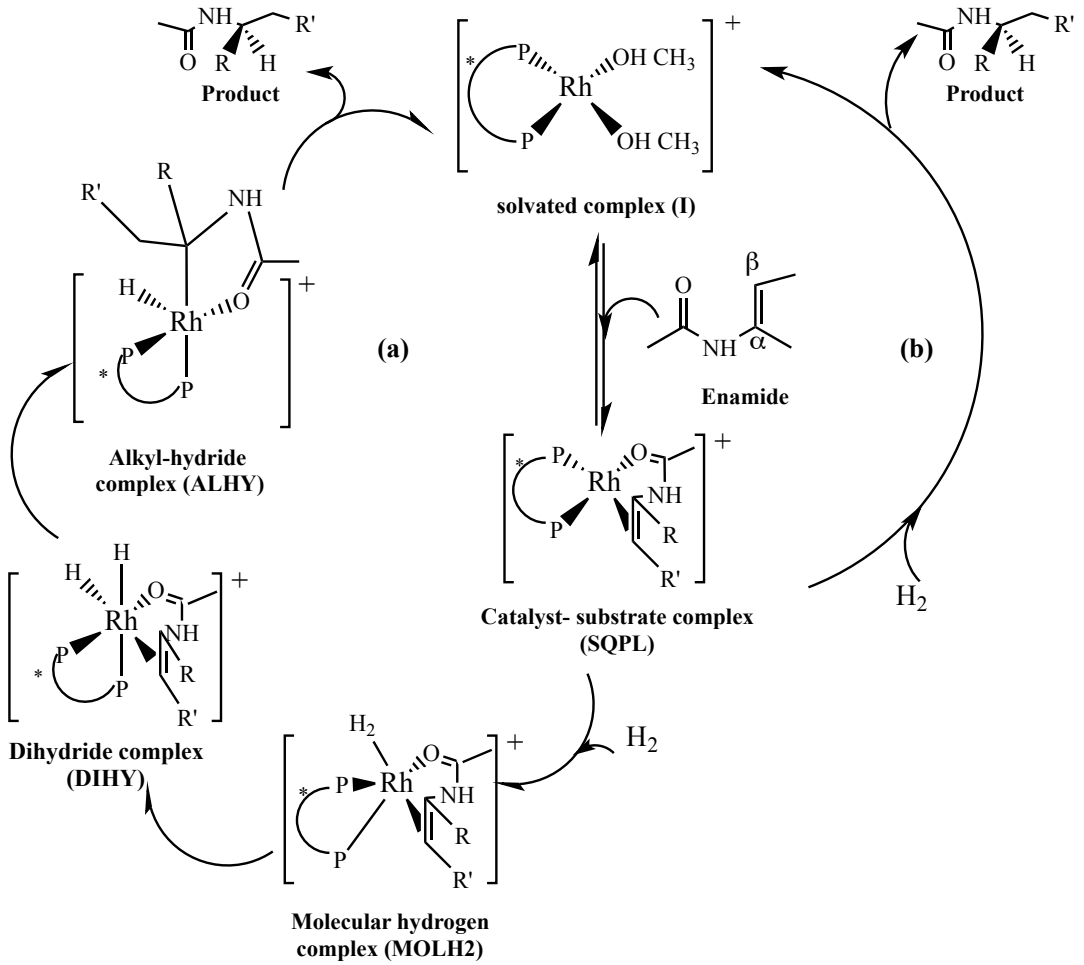

Scheme 1 : Mechanism of Chiral diphosphine rhodium-catalyzed hydrogenation of enamides: (a) mechanism including all elementary steps used for the DFT approach, (b) Simplified mechanism used in the experimental kinetic approach

The identification of the intermediates and the kinetic studies showed that the enantioselectivity is determined by the ratio of the rate constants of the H_2 oxidative addition for both diastereomeric pathways and by the ratio of the SQPL complex[9]. Most often, the least stable catalyst-substrate complex is the most reactive towards hydrogen, which is expressed by the major/minor concept[8a,] corresponding to three inequalities[9]. However, in some cases, depending on the substrate nature and on the chiral ligands, the major oxidative addition product comes from the most stable diastereoisomer, following the so-called lock and key concept[10].

To validate such a mechanism, a thorough theoretical study has been done by Landis *et al.*[6e,f] These authors have also considered the influence of the substrate substituents on the enantioselectivity and on the reactivity of the intermediates. They provided insight into the α-

substituents effect in the enamide hydrogenation, and demonstrated the confluence of both electronic and steric effects in controlling the stereochemistry.[10] A recent work indicates that the first hydride transfer depends on the electronic properties of the α- and β-substituents (see Scheme one for definition), which can induce a mechanistic change.[11]

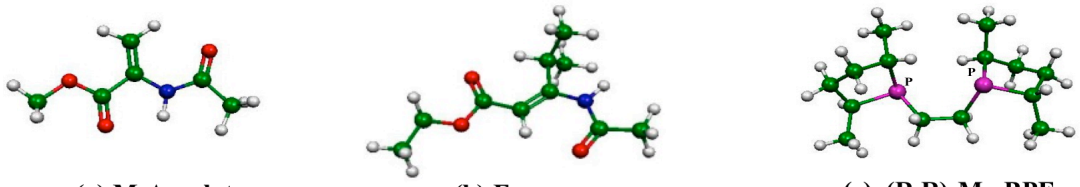

(a) M-Acrylate **(b) E-emap** **(c) (R,R)-Me-BPE**

Figure 2 : Structure of the substrates and of the chiral ligand

In this work, we focus our attention on the two enamide systems cited above for which the hydrogen pressure shows opposite effect on the enantiomeric excess. Our aim was to pinpoint the origin of this behaviour, through the contribution of experiments and of theoretical studies of the most important steps of the hydrogenation reaction, using DFT calculations. We have successively studied the oxidative addition of H_2 and the first hydride transfer, for the substrates methyl-2-acetamidoacrylate (M-acrylate) and ethyl-4-methyl-3 acetamido-2-propanoate (E-emap) and for the C_2-symmetric chiral ligand 2-[(2R,5R)-2,5-dimethylphospholan-1-yl]ethyl ((R, R)-Me-BPE) (R, R)-Me-BPE (see Figure 2). The final reductive elimination has not been considered since this step has no impact on the enantiomeric excess. Effectively, if the first attack of H takes place at the chiral carbon C_α (linked to N), the final enantiomer is fixed by the configuration around C_α in the alkyl complex (ALHY, alhy). If the first addition of H occurs at the non prochiral carbon C_β, C_α remains bound to the metal in the alkyl complex and the configuration obtained by the reductive elimination is imposed at C_α.

Concerning the dependence with the H_2 pressure, Landis et al. proposed an exhaustive experimental kinetic study, considering the two available steps, the formation of the initial complex and the oxidative addition of hydrogen[6d]. To find the origin of this dependence, they focused particularly on the extreme cases, a very small and a very high hydrogen pressure, to simplify the equations. For our part, in order to compare our two systems in a previous experimental work, we have also performed a kinetic study based on the same steps[4]. Unfortunately, that study did not allow the determination of all the kinetic constants.

In the present article, we expose the results of the theoretical study done on the same catalytic systems. The interest of the study rests on the characterization of all the intermediates and the determination of the energy barriers of all the elementary steps, which allow their use in the kinetic simulation with the hope that the step responsible for the pressure effect will be found.

Methodology:

The calculations were based on density functional theory (DFT) and were performed with the Gaussian code.[13] The Becke's three-parameter hybrid functional (B3)[14], and the Lee, Yang, and Parr correlation functional (LYP)[15] were used for all the calculations steps. In fact, the B3LYP method shows good performances in transition metal studies, both for geometry optimization and energy calculations.[16] A comparison of methods is given in the Supporting Information for the energy difference between diastereoisomer complexes and their geometries. The Dunning-Huzinaga valence double-ζ basis set was used with polarization d functions on C, N and O (D95V*) and polarization p functions on the hydrides (D95V**). Hay and Wadt effective core potentials have been used for Rh and P with LANL2DZ basis set.[17] All the structures have been fully optimized at this level.

Transition states geometries were found via the quasi-Newton algorithms[18] QST2 and QST3, and in some cases, the intrinsic reaction coordinate (IRC)[19] method leading to the corresponding energy minima has been used. All transition states were characterized by vibrational frequency calculations. Free energies were obtained through a thermo-chemical analysis, using the thermal correction to Gibbs free energy as reported by GAUSSIAN. This takes into account zero-point effects, thermal enthalpy corrections, and entropy. All energies reported in this paper have been calculated for gas-phase reactions at T = 298K and P = 1atm. For some structures, the calculations have been also performed in the presence of a solvent, methanol (ε=32.63 D), by using the Polarisable Continuum Model (PCM).[20]

Results and discussion

1- Reaction pathways

A. Formation of the square-planar cationic [Rh ((R,R)-Me-BPE)-(enamide)]$^+$ complex.

The chiral rhodium complex environment obtained by coordination of the chiral (R,R)-Me-BPE ligand can be represented according to the quadrants diagram[21] given on Figure 3. The phospholane methyl groups of (R,R)-Me-BPE can be axial or equatorial. We have chosen the equatorial orientation that is the less cumbersome. If the substrate coordinates in front of the metal, the equatorial groups at the bottom on the right and at the top on the left (labelled "front") are directed towards the site of coordination and create a steric congestion in the region that they occupy (grey quadrants on Figure 3).

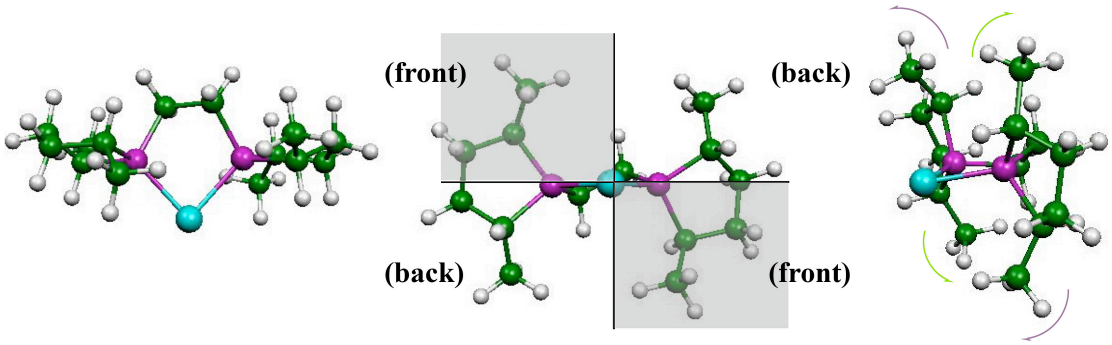

Figure 3 : Chiral ligand coordination to the rhodium

The substrate approaches the metal to minimize the steric interactions with these equatorial groups. It binds to the rhodium catalyst complex through the C=C bond and the O atom of the amide, and according to the binding face re or si, two diastereoisomeric square planar catalyst-enamide complexes (SQPL in Scheme 1) are formed as shown in Figure 4. In the following, they will be called major (**MAJ)** and minor (**MIN),** based on their relative energy. Due to the flexibility of the carbon chain of the ligand, two conformers exist for each SPQL complex. In the case of M-acrylate, these conformers have been calculated for both MAJ and MIN. The free energy difference between the conformers is 7 kJ.mol^{-1} for the former and 5 kJ.mol^{-1} for the latter. An interconversion barrier of 21 and 26 kJ.mol^{-1} is calculated for MAJ and MIN, respectively. The most stable conformers are shown on Figure 4a. They exhibit the same conformation as that of complex [(COD)Rh((R,R)-Me-BPE)]$^{+}$$SbF_6^{-}$ determined by X-Ray crystallography[22]. For the sake of simplicity and for saving computational time, we have only considered the more stable conformer in the following.

MAJ is calculated lower in energy than **MIN** by 11 kJ.mol^{-1} and 12 kJ.mol^{-1} for M-acrylate and E-emap, respectively. In fact, since the substituents on the double bond are different in the two substrates, **MAJ** and **MIN** do not correspond to the same binding face for M-acrylate and E-emap. That means that, for M-acrylate, the hydrogenation of MAJ will yield the S product while, for E-emap, MAJ is on the pathway leading to the R product.

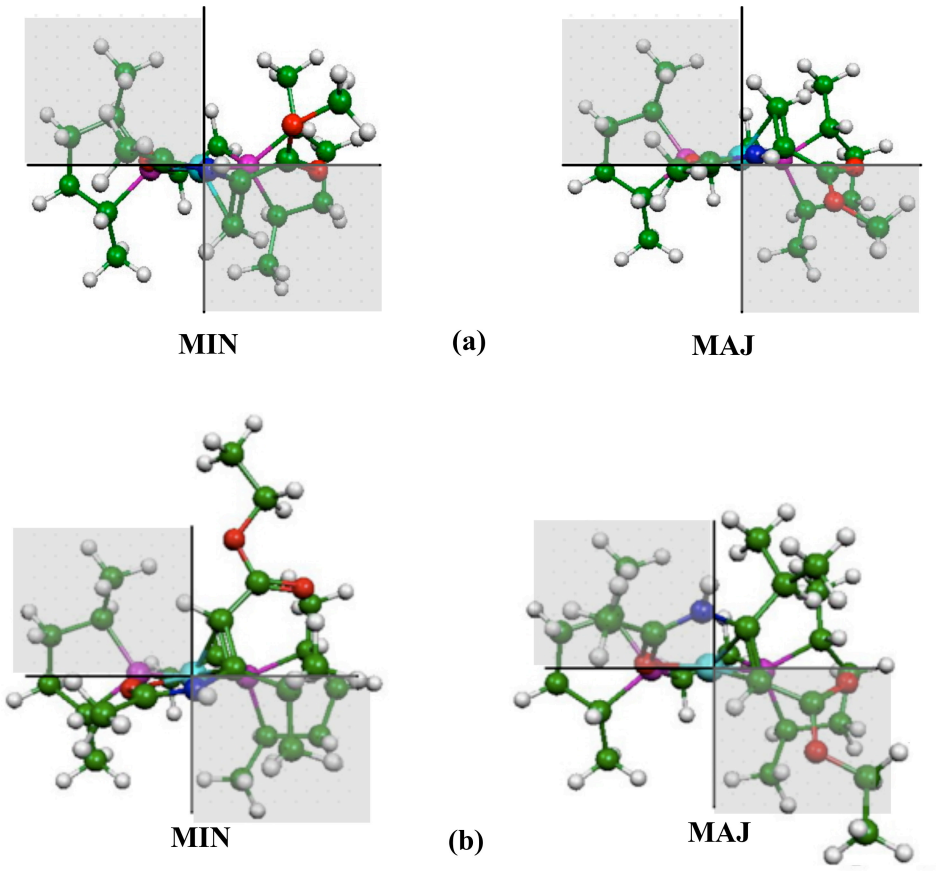

Figure 4 : structure of metal-substrate square-planar diastereomers: (a) M-acrylate; (b) E-emap

The geometrical parameters and the relative energies of the diastereoisomers are discussed in details in the SI.

B. Hydrogenation steps

The hydrogenation of the two diastereoisomeric square planar complexes **MAJ** and **MIN** leads to two catalytic cycles. In the following, the names of the intermediates and transition states for the MAJOR channel will be in capitals, whereas lower case labels will denote the minor manifold.

According to previous theoretical studies[23,6e], four mechanistic pathways have been identified for H_2 addition, which differ by the approach and orientation of H_2 relative to the square-planar catalyst-substrate complex. The notation given by Landis and co-workers for these pathways (**A**, **B**, **C** and **D)** is kept in the present work. Following their work, we have retained pathways **A** and **C** for the present study, since they were found to be the best. The

various steps of these pathways are described in the SI. The geometry of all the intermediates and transition states are given as well as the electronic energies.

As far as these energies are considered, the analysis of the results for the M-acrylate substrate shows that, for the major and minor cycles, the highest energy TS along the pathway **C** or **c**, **DIHY$^{\#}$-C** or **dihy$^{\#}$-c** for the migratory insertion of the olefin, are less stable than the highest energy TS for pathways **A** or **a**, by 22 and 40 kJ.mol^{-1}, respectively (SI, Table S3). Hence, for M-acrylate, pathway **A or a** is favored, i.e. the hydrogen attack takes place at the opposite side of the amide group. In the case of E-emap, the behaviour is inverted and the **DIHY$^{\#}$-A** or **dihy$^{\#}$-a** TS are the highest (SI, Table S5). Therefore, in the case of E-emap, pathway **C** is favoured for both the major and the minor cycles.

2- Reactivity and kinetics

A. Free energy diagrams

The calculation of the Gibbs free energies at 298K and for a pressure of 1 atm yields the profiles shown in Figures 5 and 6. According to the structures of the diastereomers, the MAJ complex leads to the S-conformer for M-acrylate, while it leads to the R-conformer for E-emap. Each diagram is divided into two parts, one corresponding to the R manifold, the other to the S manifold. For the M-acrylate substrate, pathway **A** has the lowest overall barriers on both cycles, whereas pathway **C** is blocked on both cycles by large barriers for the migratory insertion forming the agostic complexes (**DIHY$^{\#}$**). One can especially underline that the agostic intermediate and surrounding TS on the minor C pathway are 70 kJ.mol^{-1} less stable that the corresponding ones on the A pathway. The distance between H and C is larger for pathway C than for pathway A (2.53 vs. 2.24 Å), which means that the path is longer and the TS is later (1.52 vs. 1.85 Å). This directs the reaction to the case where the oxidative H_2 addition is less favoured (pathway A), with a TS higher by 4 kJ.mol^{-1} on the minor manifold, and by 17 kJ.mol^{-1} on the major one. As a matter of fact, the highest TS along pathway A corresponds to the oxidative addition both on the major and minor manifolds, and olefin insertion appears as a kinetically very easy elementary step, in line with the results of Landis[6e]. The situation is different with E-emap, where pathway **C** is preferred because of the higher barriers on pathway **A** at **DIHY$^{\#}$** transition state. In this case, the highest TS on the pathway corresponds to the olefin migratory insertion with a large corresponding barrier.

The comparison of these profiles confirms the results obtained with the electronic energies. The only difference is that in terms of Gibbs free energy, the transition states localised before for the formation of the molecular hydrogen complexes (MAJ-$H_2^{\#}$ and min-$H_2^{\#}$) are no longer transition states in the case of M-acrylate and hence, **$MOLH_2$** is no longer a stable intermediate. For E-emap in opposite, **$MOLH_2$** where the C=C bond is decoordinated remains a local minimum reached via a transition state (see Figure 6). This means that the reaction does not follow exactly the same pathway depending on the substrate. For the four pathways of M-acrylate, the hydrogen molecular complex does not exist and the hydrogenation is dissociative, leading directly to the dihydride. For E-emap, the hydrogenation is first associative and the **$MOLH_2$** complexes are real intermediates. These species are particularly stable because of the easy decoordination of the C=C bond that allows the approach of H_2. In the case of M-acrylate, the decoordination is not enough stabilizing to be a favoured pathway. In the case of E-emap along the **MIN-a** pathway, an intermediate **$MOLH_2$** with the C=C double coordinated to Rh can also be obtained as a shallow minimum. The transition state leading to it is much lower than the one leading to the **$MOLH_2$** species with the decoordinated C=C bond (70 vs. 102 kJ/mol).

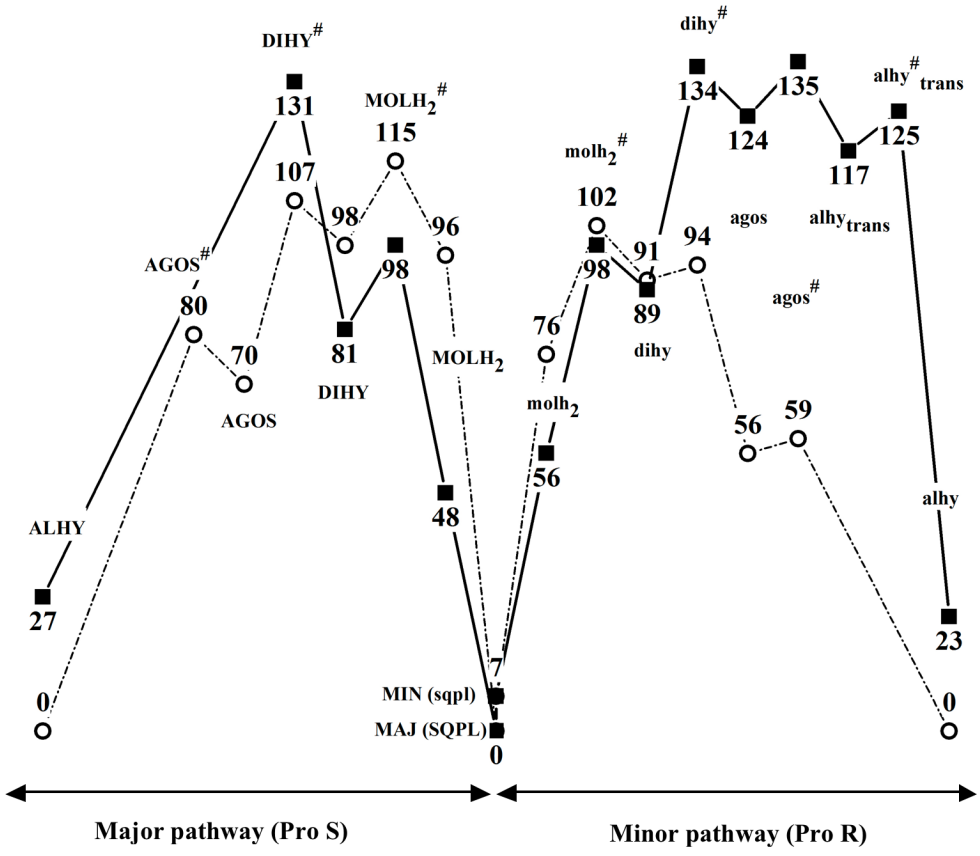

Figure 5: Free energies (kJ.mol^{-1}) for the reaction of MIN and MAJ corresponding to M-acrylate with H_2 over pathways A (○) and C (■).The energy reference is that of MAJ+H_2

All the conversions of the square planar complexes into hydrogen complexes are endergonic, but the range of the free energies is higher with the M-acrylate substrate, (from 81 to 98 kJ.mol^{-1}) than with E-emap (from 26 to 66 kJ.mol^{-1}). Furthermore, for the two substrates, the minor pathway gives the lowest energy transition state, with a difference of ca. 13 kJ.mol^{-1} compared to the corresponding one of the major pathway. Only the two preferred reaction pathways will be considered in the following discussion: pathway A for M-acrylate and pathway C for E-emap.

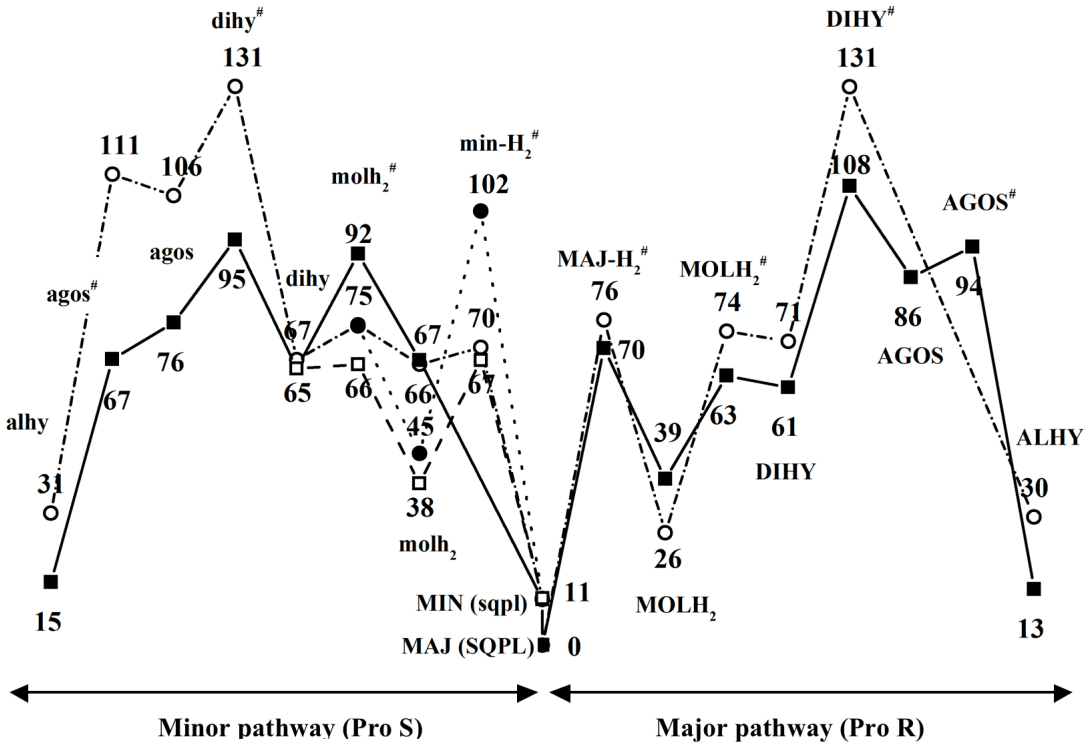

Figure 6 : Free energies (kJ.mol^{-1}) for the reaction of MIN and MAJ corresponding to E-emap with H_2 along pathways A (○,● (CCdec)) and C (■,□(CCdec)). The energy reference is that of MAJ+H_2

Up to this point, we considered the reaction from the square-planar complex. However, the formation process of this complex by coordination of the substrate E to the starting solvated complex I and decoordination of two methanol molecules (see scheme 1) should also be taken into account. This step has rarely been considered in the mechanistic studies already published. To our knowledge, only Gridnev *et al.* have addressed this issue[6h,i]. Nevertheless, the geometry optimisation for all starting species (methanol, substrate, solvated complex, intermediates) and the calculation of the vibrational frequencies provides the free energies and the three equilibrium constants (K_1^R, K_1^S, K_{DIAS}). The formation of all square-

planar complexes (MAJ and MIN) is an exothermic (except for the minor one derived from E-emap) and exergonic reaction in normal conditions, (i.e. for M-acrylate: ΔH_{MAJ} = -23 kJ.mol^{-1}; ΔG_{MAJ}= -52 kJ.mol^{-1}; ΔH_{MIN} = -13 kJ.mol^{-1}; ΔG_{MIN}= -44 kJ.mol^{-1} and for E-emap: ΔH_{MAJ} = -4 kJ.mol^{-1}; ΔG_{MAJ}= -22 kJ.mol^{-1}; ΔH_{MIN}=8 kJ.mol^{-1}; ΔG_{MIN}= -11 kJ.mol^{-1}1). The relative order of the two diastereoisomer is the same when entropy is taken into account; for example in the case of M-acrylate: $\Delta H_{MIN-MAJ}$ = 11 kJ.mol^{-1}; $\Delta G_{MIN-MAJ}$= 8 kJ.mol^{-1}.

Considering Figures 5 and 6, we can conclude that the oxidative addition, for M-acrylate, is an irreversible reaction in the preferred pathway because the insertion of the carbon into Rh-H to form the agostic structure has a lower barrier than the reductive elimination of H_2 from the dihydride to the molecular hydrogen complex. On the contrary, for E-emap, the oxidative addition can be reversible and only the migratory insertion from the dihydride complex to the alkyl-hydride is irreversible. The lowest transition states for M-acrylate and E-emap are globally obtained along the minor manifold. Hence, the least stable enamide-catalyst complexes show a considerably smaller barrier than the most stable ones.

All the energies presented above have been calculated in gas phase. In order to get closer correspondence with the experimental data, the impact of solvation has been checked on the enantio-determining steps for each substrate, and on the formation steps of the square planar complexes. No important change in the conclusions has been found.

B. Kinetic simulations

In order to go further in the understanding of the catalytic reaction and to get more insights on the effect of hydrogen pressure, a detailed micro-kinetic model is proposed below, based on the mechanism obtained from quantum chemistry. The catalytic cycles we considered are summarized in Scheme 2, following the steps determined by the DFT calculations, as shown in Figures 5 and 6.

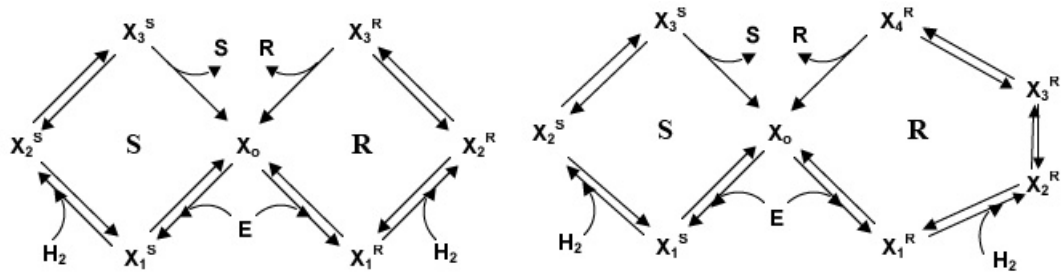

Scheme 2: Theoretical mechanism according to the DFT calculations. X_0 is the starting solvated Rh complex (I in Scheme 1) and E represents the enamide. On the left: M-acrylate, on the right: E-emap.

That model is more detailed than the one initially proposed in the literature since the DFT calculations allow the determination of the kinetics parameters for a more extended network of elementary steps. Some intermediates formed with a negligible barrier such as alhy-trans are not considered in order to simplify the model. The last elementary step of alkylhydride formation was associated to the irreversible formation of the enantiomeric product[6i]. The considered elementary steps are not the same for the two substrates. There are four steps in the case of M-acrylate and the S pathway of E-map and five steps for the R pathway of E-emap. Hence, the kinetic model includes 14 kinetic constants for M-acrylate, k_i and k_{-i}, (i=1, 2, 3 and 4) i.e. 7 constants for each R and S cycle, and 16 constants for E-emap since the R pathway shows two more steps in that case. Except for the first step, these constants were calculated within the transition state theory according to the formalism proposed by Eyring[24], as given by eq. 1, where k_B is the Boltzmann constant, T the absolute temperature, and h the Planck's constant. $\Delta G^{\#}_i$ is the activation free energy for each step. The standard concentration (c° =1 mol.L^{-1}) was considered. In the case of the first step, only the Gibbs reaction energy is determined, which allows the calculation of the equilibrium constants (K_{1R} and K_{1S}) and hence of the ratio of the two corresponding kinetic constants k_1 and k_{-1} (eq. 2). One parameter is hence missing to fully determine k_1 and k_{-1} for each R and S cycle.

eq. 1 $$k_i = \frac{k_B T}{hc^0} e^{-\Delta G_i^{\#}/RT}$$

eq. 2 $$K = \frac{k_i}{k_{-i}} = e^{-\Delta G^0/RT}$$

Table 1 reports all kinetic parameters (k_i, k_{-i}, K, **ΔG°, $\Delta G^{\#}$**) obtained from the DFT calculations.

Table 1: Free energy change of a reaction (ΔG°) or standard Gibbs energy of activation ($\Delta G^{\#}$) and respectively equilibrium or kinetic constant given by theoretical computation at T=300K and P= 1 atm.

Elementary step			M-acrylate			E-emap		
				ΔG° (kJ.mol^{-1})	**K**		**ΔG° (kJ.mol^{-1})**	**K**
I+A	⇆	**$(SQPL)_R$**	**(1R)**	-44	$5\ 10^{7}$	**(1R)**	-22	$6\ 10^{3}$
I+A	⇆	**$(SQPL)_S$**	**(1S)**	-51	10^{9}	**(1S)**	-11	80
				$\Delta G^{\#}$ (kJ.mol^{-1})	**k**		**$\Delta G^{\#}$ (kJ.mol^{-1})**	**k**
$(SQPL)_R$	→	**$(MOLH_2)_R$**		-	-	**(2R)**	70	4.1
$(MOLH_2)_R$	→	**$(SQPL)_R$**		-	-	**(-2R)**	31	$2.5\ 10^{7}$
$(SQPL)_R$	→	**$(DIHY)_R$**	**(2R)**	95	$1.8\ 10^{-4}$		-	-
$(DIHY)_R$	→	**$(SQPL)_R$**	**(-2R)**	11	$7.6\ 10^{10}$		-	-
$(SQPL)_S$	→	**$(MOLH_2)_S$**		-	-	**(2S)**	56	$1.1\ 10^{3}$
$(MOLH_2)_S$	→	**$(SQPL)_S$**		-	-	**(-2S)**	30	$3.7\ 10^{7}$
$(SQPL)_S$	→	**$(DIHY)_S$**	**(2S)**	115	$5.9\ 10^{-8}$		-	-
$(DIHY)_S$	→	**$(SQPL)_S$**	**(-2S)**	17	$6.9\ 10^{9}$		-	-
$(MOLH_2)_R$	→	**$(DIHY)_R$**		-	-	**(3R)**	24	$4.1\ 10^{8}$
$(DIHY)_R$	→	**$(MOLH_2)_R$**		-	-	**(-3R)**	2	$2.8\ 10^{12}$
$(MOLH_2)_S$	→	**$(DIHY)_S$**		-	-	**(3S)**	29	$5.6\ 10^{7}$
$(DIHY)_S$	→	**$(MOLH_2)_S$**		-	-	**(-3S)**	1	$4.2\ 10^{12}$
$(DIHY)_R$	→	**$(AGOS)_R$**	**(3R)**	3	$1.9\ 10^{12}$	**(4R)**	47	$4.1\ 10^{4}$
$(AGOS)_R$	→	**$(DIHY)_R$**	**(-3R)**	38	$2\ 10^{6}$	**(-4R)**	22	$9.2\ 10^{8}$
$(DIHY)_S$	→	**$(AGOS)_S$**	**(3S)**	9	$1.7\ 10^{11}$		-	-
$(AGOS)_S$	→	**$(DIHY)_S$**	**(-3S)**	37	$2\ 10^{6}$		-	-
$(DIHY)_S$	→	**S**				**(4S)**	30	$3.7\ 10^{7}$
$(AGOS)_R$	→	**R**	**(4R)**	3	$1.9\ 10^{12}$	**(5R)**	8	$2.5\ 10^{11}$
$(AGOS)_S$	→	**S**	**(4S)**	10	$1.1\ 10^{11}$			

From the knowledge of all the kinetic constants, the enantiomeric excess can be expressed as a function of the hydrogen pressure. The formula is given in eq. **3**, with a, b, α, and β having complicated expressions based on combinations of the kinetic constants. The details of the kinetic model can be found in the Supplementary Information.

eq. 3 $$ee = \frac{a[H_2] + b}{\alpha[H_2] + \beta}$$

A simulation was performed by minimizing the difference between the theoretical and experimental enantiomeric excess values over the range of hydrogen pressure considered for the experiments (2-41 bar) (method of least squares) in order to determine the two missing parameters fixing k_1 and k_{-1} for the R and S cycles. The corresponding theoretical and experimental profiles are given in Figure 7. This figure reveals the perfect agreement between the experimental and the theoretical results and shows the robustness of the theoretical model, knowing that only two parameters are fitted.

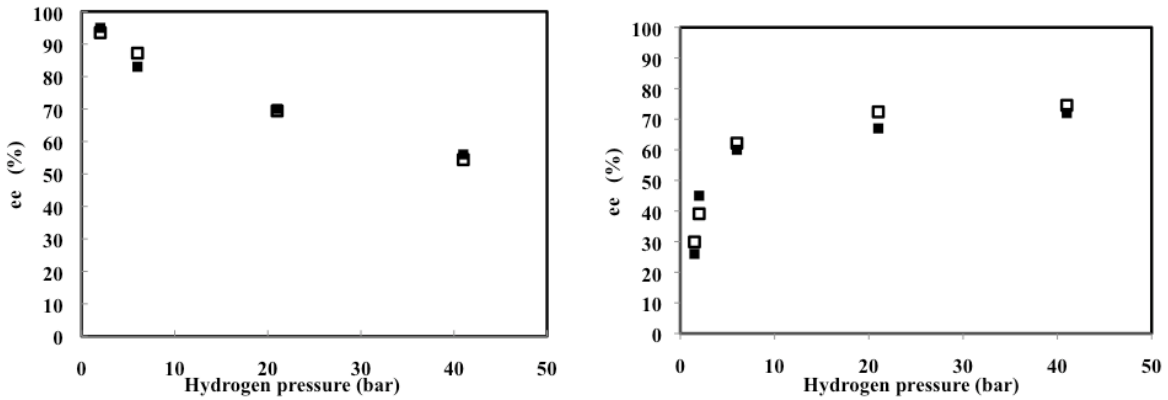

Figure 7 : Hydrogen pressure and enantiomeric excess dependency: similarity between experimental results (■) and theoretical models (□). M-acrylate on the left; E-emap on the right.

These simulations allowed the determination of the values of k_1 and k_{-1} for each substrate. They are given in Table 2. Hence, the kinetic constants of all the elementary steps are now known.

Table 2: kinetic constants k_1 and k_{-1} from the theoretical kinetic model

	(i)	(1)	(-1)
M-acrylate	k_{iR}	$4.2\ 10^{1}$	$8.6\ 10^{-7}$
	k_{iS}	$4.5\ 10^{1}$	$4.5\ 10^{-8}$
E-emap	k_{iR}	$2.0\ 10^{-4}$	$3.3\ 10^{-8}$
	k_{iS}	$2.6\ 10^{-5}$	$3.3\ 10^{-7}$

C. Discussion

We have noted before that the comparison of the barriers in Figures 5 and 6 leads to the conclusion that the minor manifold should the preferred one, yielding the R product in the case of M-acrylate and the S product in the case of E-emap. The kinetic simulation leads to an opposite conclusion for E-emap. Nevertheless, there is no incoherence between the two approaches. In the first qualitative approach indeed, the step of formation of the SQPL

complex is not considered nor the H_2 pressure. Following equation 3, ee is equal to b/β if the H_2 pressure is zero. With the values obtained by the simulation (cf Supplementary Information), ee is equal to -99%. Moreover the theoretical curve fitting the experimental results (see Figure S7 in SI) gives negative ee values for low H_2 pressures (below 0.7 bar) and a product with S configuration, in agreement with the diagram of Figure 6. There is thus a change in the absolute configuration of the major product when the pressure of H_2 increases. This illustrates that a complete kinetic model, including the step of the SQPL complex formation, is necessary to account for the experimental results. There is a compromise between the formation rate of the SQPL complex and its reaction rate to give the hydrogenated product.

The reaction rates can be expressed as a function of the hydrogen pressure (see Supplementary Information). The expressions are complicated but the ratio r_R/r_S of the R and S product formation rates can be easily calculated. These ratios are plotted in Figure 8. These graphs are very similar to the experimental ones shown in Figure S8 in the Supplementary Information.

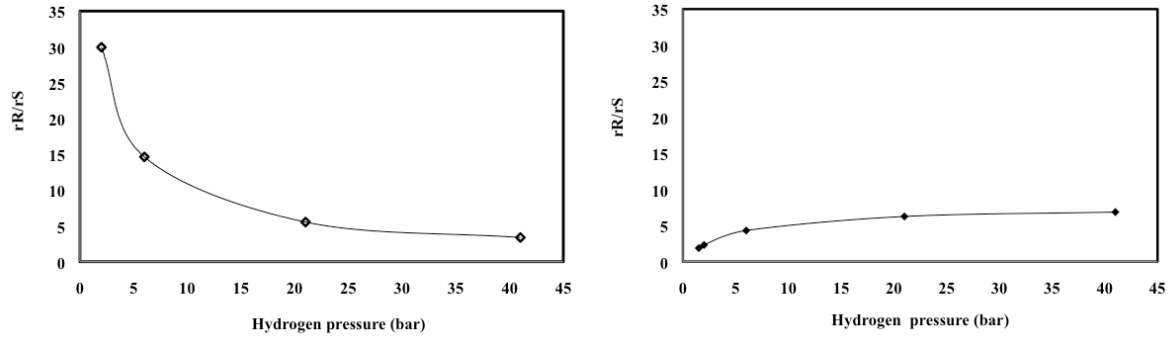

Figure 8: Evolution of the R versus S formation rate ratio obtained by the calculations as a function of the hydrogen pressure. M-acrylate on the left; E-emap on the right.

If one assumes that $r = kP_{H2}^{a}$, then $Ln(r) = Ln(k) + a\ Ln(P_{H2})$. The corresponding graphs obtained with the experimental values for M-acrylate and E-emap are given in Figure 9.

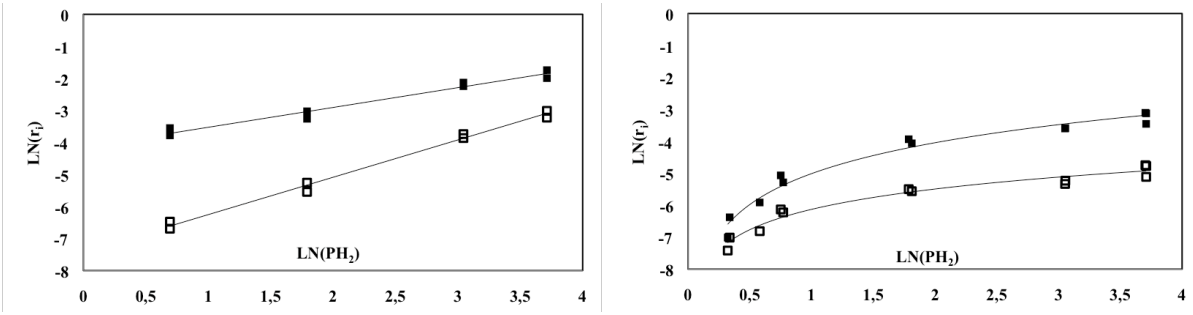

Figure 9 : Experimental evolution of the R versus S formation rate as a function of hydrogen pressure. (■) corresponds to R and (□) corresponds to S. On the left: M-acrylate; on the right: E-emap.

The slopes of the lines are different for the R and the S isomer. In the case of M-acrylate, r_S increases more rapidly than r_R when the pressure increases, which explains that rR/rS and ee decrease when P_{H2} increases, as illustrated in Figures 7 and 8. For E-emap in contrast, r_R increases slightly more rapidly than r_S, which results in an increase of rR/rS and ee. The difference between the slopes of the R and S lines is larger in the case of the M-acrylate and rR/rS varies more rapidly for M-acrylate than for E-emap. The difference between the initial reaction rates of the R and the S isomers (when P_{H2} tends to zero) is far larger for the M-acrylate than for E-emap, which means that the formation of isomer R is largely preferred for the former (ee =95%), while it is less predominant for the latter (ee=26%). Two steps of the mechanism can contribute to this difference. First, the formation of the SQPL starting complex is much slower for E-emap since the k_i constants are smaller. Secondly, the largest barrier in the R pathway for M-acrylate is lower than the corresponding one for E-emap (95 vs. 108 kJ/mol). The two effects add. They are related with the bulkiness of the substituents of E-emap compared to those on M-acrylate that hinders both the coordination of the substrate and the approach of hydrogen on the two complex faces, which implies a smaller differentiation of these faces.

The foregoing results show that the hydrogenation of M-acrylate and E-emap does not follow the same mechanism. In the case of M-acrylate, the minor square-planar substrate-metal complex leads to the product, according to the major/minor concept. In the case of E-emap in contrast, the product comes from the major starting complex, according to the lock-and-key concept. However, as we have noticed before, the minor complex for M-acrylate and the major complex for E-emap correspond to the same orientation of the double bond relatively to the Rh-diphosphine moiety (see Figure 4). Hence, it seems that this orientation plays a determinental role in the enantioselectivity.

In order to go further in the interpretation, it would be interesting to know which step is responsible for the trends we have discussed above. For that purpose, we have tested how much the rate ratio or ee is changed when each kinetic constant is successively increased or decreased by 10% in order to determine the enantioselectivity determining step. In fact, for both M-acrylate and E-emap, it was found that several constants and, hence, several steps play a role and no clear conclusion could be drawn. This is easily understood when the literal expression given for ee in Supplementary Information is considered. ee reads as a complex combination of all the kinetic constants from which none stands out. Similarly, the variation direction of ee with the H_2 pressure cannot be related to one step in particular. This can be verified literally by studying the sign of the derivative of ee with respect to the concentration of hydrogen. In the case of M-acrylate for instance, this is equivalent to studying the sign of eq. **4** (see SI).

eq. 4:

$$\text{Sign}(\text{dee}/\text{d}[H_2]) = \text{sign}\left(1 - \frac{k_{2R}k_{3R}k_{4R}k_{5R}k_{-1S}(k_{3S}k_{4S} + k_{-2S}k_{4S} + k_{-2S}k_{-3S})}{k_{2S}k_{3S}k_{4S}k_{-1R}(k_{5R}(k_{3R}k_{4R} + k_{-2R}k_{4R} + k_{-2R}k_{-3R}) + k_{-2R}k_{-3R}k_{-4R})}\right)$$

or sign of

$$k_{1R}k_{1S}\left[k_{2S}k_{3S}k_{4S}k_{-1R}(k_{3R}k_{4R} + k_{-2R}k_{4R} + k_{-2R}k_{-3R}) - k_{2R}k_{3R}k_{4R}k_{-1S}(k_{3S}k_{4S} + k_{-2S}k_{4S} + k_{-2S}k_{-3S})\right]$$

Since all constants are positive, this sign depends on the numerical values of the constants, except k_{1R} and k_{1S}. Hence, it is not possible to find any simple relation between the constants to determine the variation direction of ee. Nevertheless, the step of formation of the square-planar complex has no influence on it. From these expressions, ee can obviously decrease or increase depending on the relative values of the kinetic constants of several elementary steps. The values of these constants depend on the nature of the catalyst and of the substrate. However, owing to the complexity of the literal expression of ee, it is impossible to determine which constants play an important role, in agreement with the tests cited just above. The arguments above explain the experimental results[3]. Indeed experimentally, cases where ee decreases and increases with $[H_2]$ are both found**.**

Conclusion

The goal of this work was to understand the variation with the hydrogen pressure of the enantioselectivity of enamide hydrogenation catalyzed by a chiral rhodium catalyst. Two

substrates with different steric and electronic properties, and showing a different behavior against the hydrogen pressure were compared by means of DFT calculations. Two pathways were studied for each molecule, starting from the two diastereoisomeric complexes resulting from the coordination of the substrate on the chiral catalyst. All the elementary steps were studied, and the transition states were characterized. The decomposition of the mechanism in several steps has shown that the hydrogenation of the starting complex can be dissociative or associative, depending on the substrate. The rate-limiting step depends also on the substrate. For M-acrylate, this step is the oxidative addition of hydrogen and for E-emap, it is the migratory insertion of the C-C double bond into the R-H bond.

Differing from most of the previous works, we have proposed a detailed kinetic model using the calculated kinetic constants, which allows the prediction of the hydrogen pressure impact. Our complete model allows us to understand why ee varies with the H_2 pressure. It underlines the key role played by the step of formation of the initial square planar complex on the experimental enantioselectivity. The formation of the R isomer for both molecules was explained by two different mechanisms following either the major/minor or the lock-and-key concept, but coming in fact from the same coordination orientation of the C=C double bond. The stereoselectivity found by the calculations was in perfect agreement with the experimental results and the calculated enantiomeric excesses were close to the experimental values. However, the complexity of the kinetic network implies that the other steps are also involved. The robustness of the theoretical model, which has been evidenced by the present study, opens the way to the investigation of systems with different ligands and substituents with the hope that the enantiomeric excess can be anticipated by a theoretical study. Moreover, the theoretical DFT calculations could help the experimentalists to assign the absolute configuration of the products obtained by this type of enantioselective hydrogenations.

Acknowledgements

Financial support was provided by the Région Rhône-Alpes and the Centre National de la Recherche Scientifique (CNRS). The authors thank the Centre Informatique National de l'Enseignement Supérieur (CINES) at Montpellier, the Institut du Développement et des Ressources en Informatique Scientifique (IDRIS) at Orsay and the Pôle Scientifique de Modélisation Numérique (PSMN) at ENS-Lyon for CPU time.

Supplementary Information are available.

References

[1] H.-U. Blaser, E. Schmidt, Asymmetric Catalysis on Industrial Scale, Wiley-VCH, **2004**; (b) S. C. Stinson, *Chem. Engineering News* **2001**, *79*, 79-97.

[2] (a) I. Ojima, T. Kogure, N. Yoda, *J. Org. Chem.* **1980**, 45, 4728-4738; (b) A. Marinetti, S. Jus, J. P. Genêt, *Tetrahedron Lett*. **1999**, 40, 8365-8368; (c) D. Heller, J. Holz, I. V. Komarov, H. J. Drexler, J. You, K. Drauz, A. Boener, *Tetrahedron: Asymmetry* **2002**, 13, 2735-2741; (d) Y. Sun, J. Wang, C. LeBlond, R. N. Landau, J. Laquirada, J. R. Sowa Jr., D. G. Blackmond, *J. Mol. Catal. A*: **1997**, 115, 495-502

[3] M. Alame, N. Pestre, C. De Bellefon, *Adv. Synth. Catal*. **2008**, 350, 898-908

[4] A. Aloui, F. Delbecq, P. Sautet, C. De Bellefon, *J. Mol. Cat. A* **2012** 363-364, 214-222.

[5] D. Heller, J. Holz, I. Komarov, H.-J. Drexler, J. You, K. Drauz, A. Börner, Tetrahedron: Asymmetry **2002**, 13, 2735-2741.

[6] (a) A. S. C. Chan, J. J. Pluth, J. Halpern, *J. Am. Chem. Soc.* **1980**, 102, 5952-5954 ; (b) J. Halpern, *Science,* **1982**, 217, 401-407 ; (c) J. Halpern, Asymmetric Synthesis ; J. D. Morrison, Ed ; Academic Press : Orlando, **1985**, 5, 41-69 ;(d) C. R. Landis, J. Halpern, *J. Am. Chem. Soc.* **1987**, 109, 1746-1754 ; (e) S. Feldgus, C.R. Landis, *J. Am.Chem. Soc.* **2000**, *122*, 12714-12727; (f) C.R. Landis S. Feldgus, *Angew. Chem. Int. Ed.* **2000**, 39, 2863-2866; (g) I. D. Gridnev, T. Imamoto, *Organometallics,* **2001,** *20,* 545-549 ; (h) I. D. Gridnev, T. Imamoto, G. Hoge, M. Kouchi, H. Takahashi, *J. Am. Chem. Soc.* **2008**, 130, 2560-2572 ; (i) I. D. Gridnev, T. Imamoto, Chem. Commun., **2009**, 7447–7464; (j) S. Mori, T. Vreven. and K. Morokuma, *Chem. Asian J.* **2006**, *1*, 391 – 403; (k) S. Feldgus and C. R. Landis, Organometallics **2001**, 20, 2374-2386.

[7] K. V. L. Crépy, T. Imamoto, *Adv. Synth. Catal.*, **2003**, 345, 79-101

[8] (a) J. M. Brown, P. A. Chaloner, *J. Chem. Soc. Chem. Commun.* **1980**, 344-346 (b) J. M. Brown, P. A. Chaloner, *Homogeneous Catalysis with Metal Phosphine Complexes* ; L. H. Pignolet, Ed ; Plenum Press : NewYork, **1980**, 137-165 (c) J. M. Brown, *Chem Soc. Rev.* **1993**, 22, 25-41

[9] T. Schmidt, Z. Dai, H.-J. Drexler, M. Hapke, A. Preetz, and D. Heller, *Chem. Asian J.* **2008**, 3, 1170 – 1180

[10] (a) D. Evans, F. E. Michael, J. S. Tedrow, K. R. Campos, *J. Am. Chem. Soc.* **2003**, *125*, 3534-3543; (b) H.-J. Drexler, W. Baumann, S. Zhang, T. Schmidt, A. Sun, A. Spannenberg, C. Fischer, H. Buschmann, D. Heller, *Angew. Chem., Int. Ed.* **2005**, *44*, 1184-1188

[11] S. Feldgus, C. R. Landis, *Organometallics* **2001**, 20, 2374-2386

[12] P. J. Donoghue, P. Helquist, O. Wiest, *J. Org. Chem.* **2007**, 72, 839-847

[13] Gaussian 03, Revision D.01, M. J. Frisch, G. W. Trucks, H. B. Schlegel, G. E. Scuseria, M. A. Robb, J. R. Cheeseman, J. A. Montgomery, Jr., T. Vreven, K. N. Kudin, J. C. Burant, J. M. Millam, S. S. Iyengar, J. Tomasi, V. Barone, B. Mennucci, M. Cossi, G. Scalmani, N. Rega, G. A. Petersson, H. Nakatsuji, M. Hada, M. Ehara, K. Toyota, R. Fukuda, J. Hasegawa, M. Ishida, T. Nakajima, Y. Honda, O. Kitao, H. Nakai, M. Klene, X. Li, J. E. Knox, H. P. Hratchian, J. B. Cross, V. Bakken, C. Adamo, J. Jaramillo, R. Gomperts, R. E. Stratmann, O. Yazyev, A. J. Austin, R. Cammi, C. Pomelli, J. W. Ochterski, P. Y. Ayala, K. Morokuma, G. A. Voth, P. Salvador, J. J. Dannenberg, V. G. Zakrzewski, S. Dapprich, A. D. Daniels, M. C. Strain, O. Farkas, D. K. Malick, A. D. Rabuck, K. Raghavachari, J. B. Foresman, J. V. Ortiz, Q. Cui, A. G. Baboul, S. Clifford, J. Cioslowski, B. B. Stefanov, G. Liu, A. Liashenko, P. Piskorz, I. Komaromi, R. L. Martin, D. J. Fox, T. Keith, M. A. Al-Laham, C. Y. Peng, A. Nanayakkara, M. Challacombe, P. M. W. Gill, B. Johnson, W. Chen, M. W. Wong, C. Gonzalez, and J. A. Pople, Gaussian, Inc., Wallingford CT, 2004.

Gaussian 09, Revision A.02, M. J. Frisch, G. W. Trucks, H. B. Schlegel, G. E. Scuseria, M. A. Robb, J. R. Cheeseman, G. Scalmani, V. Barone, B. Mennucci, G. A. Petersson, H. Nakatsuji, M. Caricato, X. Li, H. P. Hratchian, A. F. Izmaylov, J. Bloino, G. Zheng, J. L. Sonnenberg, M. Hada, M. Ehara, K. Toyota, R. Fukuda, J. Hasegawa, M. Ishida, T. Nakajima, Y. Honda, O. Kitao, H. Nakai, T. Vreven, J. A. Montgomery, Jr., J. E. Peralta, F. Ogliaro, M. Bearpark, J. J. Heyd, E. Brothers, K. N. Kudin, V. N. Staroverov, R. Kobayashi, J. Normand, K. Raghavachari, A. Rendell, J. C. Burant, S. S. Iyengar, J. Tomasi, M. Cossi, N. Rega, J. M. Millam, M. Klene, J. E. Knox, J. B. Cross, V. Bakken, C. Adamo, J. Jaramillo, R. Gomperts, R. E. Stratmann, O. Yazyev, A. J. Austin, R. Cammi, C. Pomelli, J. W. Ochterski, R. L. Martin, K. Morokuma, V. G. Zakrzewski, G. A. Voth, P. Salvador, J. J. Dannenberg, S. Dapprich, A. D. Daniels, O. Farkas, J. B. Foresman, J. V. Ortiz, J. Cioslowski, and D. J. Fox, Gaussian, Inc., Wallingford CT, 2009.

[14] Becke, A. D. *Phys. Re*V. *A* **1988**, *38*, 3098-3100

[15] Lee, C.; Yang, W.; Parr, R. G. *Phys. Re*v. *B* **1988**, *37*, 785-789.

[16] T. Sperger, I. A. Sanhueza, I. Kalvet, Franziska Schoenebeck, Chem. Rev. **2015**, *115*, 9532..

[17] (a) P. J. Hay, W. R. Wadt, *J. Chem. Phys.* **1985**, *82*, 299. (b) W. R. Wadt, P. J. Hay, *J. Chem. Phys.* **1985**, *82*, 284. (c) P. J. Hay, W. R. Wadt, *J. Chem. Phys.* **1985**, *82*, 270.

[18] C. Peng, H. B. Schlegel, *Isr. J. Chem.* **1993**, 33, 449

[19] (a) K. Fukui, *Acc. Chem. Res.* **1981**, *14*, 363. (b) C. Gonzales, H. B. Schlegel, *J. Phys. Chem.* **1990**, *94*, 5523. (c) C. Gonzales, H. B. Schlegel, *J. Chem. Phys.* **1991**, *95*, 5853.

[20] J. Tomasi, *Chem. Rev.*, **1994**, 94, 2027.

[21] W. S. Knowles, *Acc. Chem. Res.* **1983**, 16 106-112

[22] M. J. Burk, J. E. Feaster, W. A. Nugent, R. L. Harlow, *J. Am. Chem. Soc.* **1993**, 115, 10125-10138.

[23] C. R. Landis, P. Hilfenhaus, S. Feldgus, *J. Am. Chem. Soc.* **1999**, 121, 8741-8754.

[24] Connors, K. A. Chemical Kinetics-The Study of Reaction Rate in Solution; John Wiley & Sons: New York, **1990**, p 200.